



Title	Glycomacrocycle-Based Azobenzene Derivatives as Chiral Dopants for Photoresponsive Cholesteric Liquid Crystals
Author(s)	Kim, Yuna; Mafy, Noushaba Nusrat; Maisonneuve, Stephane; Lin, Chaoqi; Tamaoki, Nobuyuki; Xie, Juan
Citation	ACS applied materials & interfaces, 12(46), 52146-52155 <a href="https://doi.org/10.1021/acsami.0c14880">https://doi.org/10.1021/acsami.0c14880</a>
Issue Date	2020-11-18
Doc URL	<a href="http://hdl.handle.net/2115/83298">http://hdl.handle.net/2115/83298</a>
Rights	This document is the Accepted Manuscript version of a Published Work that appeared in final form in ACS applied materials & interfaces, copyright c American Chemical Society after peer review and technical editing by the publisher. To access the final edited and published work see <a href="https://pubs.acs.org/doi/10.1021/acsami.0c14880">https://pubs.acs.org/doi/10.1021/acsami.0c14880</a> .
Type	article (author version)
File Information	ACS Appl Mater Interf GM-azo CLC HUSCAP.pdf



[Instructions for use](#)

# Glycomacrocycle-based azobenzene derivatives as chiral dopants for photoresponsive cholesteric liquid crystals

*Yuna Kim,<sup>a\*</sup> Noushaba Nusrat Mafy,<sup>a</sup> Stéphane Maisonneuve,<sup>b</sup> Chaoqi Lin,<sup>b</sup> Nobuyuki Tamaoki,<sup>a\*</sup> and Juan Xie<sup>b\*</sup>*

<sup>a</sup>Research Institute for Electronic Science, Hokkaido University, N-20, W-10, Kita-Ku, Sapporo, 001-0020, Japan

<sup>b</sup>Université Paris-Saclay, ENS Paris-Saclay, CNRS, Photophysique et Photochimie Supramoléculaires et Macromoléculaires, Institut d'Alembert, 4 avenue des sciences, 91190 Gif-sur-Yvette, France

\*E-mail: ykim@es.hokudai.ac.jp; tamaoki@es.hokudai.ac.jp; joanne.xie@ens-paris-saclay.fr

## **ABSTRACT**

We demonstrate photoresponsive cholesteric liquid crystals (CLCs) doped with glycomacrocylic azobenzene derivatives, which exhibit large conformational changes, providing dynamic control of helical superstructures in response to a light stimulus. An unprecedented shortening of the helical pitch length and the empowerment of helical twisting power up to 500% are observed upon *trans* (*E*) to *cis* (*Z*) photoisomerization. Light-driven dynamic helix twisting and untwisting behavior affords the first example of glycomacrocylic

azobenzenes-based CLCs which can drive the mechanical movement of micro-objects. Two modes of rotations - two-directional or one-directional rotational motion (crankshaft mode) - are realized. In particular, the latter mode based on the reversible cholesteric texture transition between homogeneous stripes and focal conics leads to the accumulation of the rotation angles achieving the amplified mechanical movements.

**KEYWORDS** : cholesteric liquid crystal, photoisomerization, glycomacrocylic azobenzene, helical twisting power, unidirectional rotation

## 1. INTRODUCTION

Photoresponsive liquid crystalline (LC) system has attracted considerable interest to a very promising area of soft photonics and mechanics.<sup>1-8</sup> Under light irradiation, it is possible to modulate or switch the orientation of LC molecules to achieve desired optical and mechanical properties of this system remotely and selectively. Especially, by introducing suitable photoresponsive chiral dopant in achiral nematic liquid crystal (NLC), self-organized chiral NLC or cholesteric liquid crystal (CLC) is formed exhibiting superstructural chirality.<sup>9-15</sup> Its helical orientation and pitch length can be dynamically controlled by light enabling the practical photonic applications for reflective displays,<sup>16-20</sup> diffraction light stirring,<sup>21,22</sup> information storage,<sup>23,24</sup> mirrorless lasing<sup>25,26</sup> as well as in molecular mechanical systems, for example, molecular switch<sup>27-34</sup> and molecular machine development.<sup>35-37</sup> Experimentally, the ability to twist or helical twisting power (HTP,  $\beta$ ) of the chiral dopant can be quantified and represented by  $\beta = (PC)^{-1}$  where  $C$  and  $P$  are the concentration of dopant and pitch of the helix, respectively.<sup>38</sup> In general, the initial and photoinduced transition in HTP value mainly determines the potential extent of CLC helix controllability such as handedness and degree of pitch length switching, which consequently limits its applications. High HTP and its

significant switching can reduce the concentration of chiral dopants avoiding undesirable changes in physical properties (e.g. viscosity, clearing point) of CLCs, which plays a significant role in optical display addressing.<sup>10,11,32,35</sup> Likewise for molecular machinery applications, photoinduced large HTP switching significantly benefits manipulation of superstructural mechanical motion by CLCs.<sup>10,11,35</sup> Furthermore, inducing higher than original HTP upon light stimulus would be favorable, as on-demand amplification of superstructural helical strain can afford much efficient and advanced control of mechanical functions in CLCs.

Lots of attempts have been challenged to develop promising CLC-based systems by tuning the molecular structures. Among the photoresponsive chiral dopants for CLCs, azobenzene-based chiral switch is considered as a very promising dopant because light-triggered geometry and polarity transition between rod-like *trans* (*E*) form (low energy, less polar) and bent shape *cis* (*Z*) form (higher energy, more polar) can effectively direct the reorganization of self-assembly of the LC molecule. Various experimental<sup>38-42</sup> and theoretical<sup>43,44</sup> studies revealed that structural rigidity, closer intramolecular photoisomerizable unit-chiral unit distance, lower conformational freedom and its large photoinduced transition of the dopant are suitable to realize higher HTP and better phototunability of the helical pitch.<sup>8-11</sup> Such molecular characteristics have been highly expected from cyclic forms, but probable examples are limited such as integrating axially chiral binaphthyl unit<sup>42,45-47</sup> or naphthalene derivatives resulting in planar chirality via cyclization<sup>9,10,17,27,35</sup> with azobenzene unit.

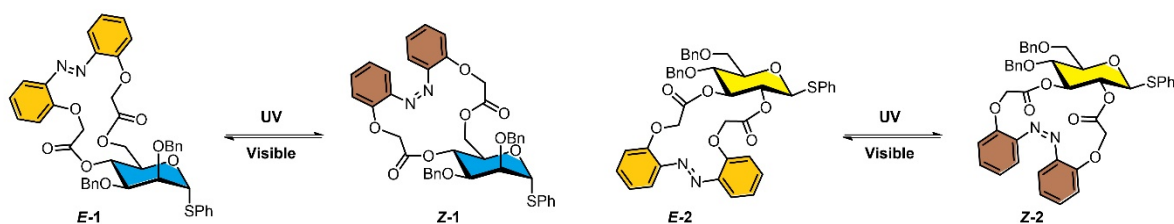
Meanwhile, realizing HTP increase under *Z*-rich state in the CLC medium is basically challenging and has been relatively unexplored. Because chirality transfer from *E* isomers to host NLC (higher HTP) is usually superior to that from *Z* isomers (lower HTP) due to intrinsic geometrical similarity of rod-shaped *E*-form and LC molecule. That is,  $E \rightarrow Z$

photoisomerization likely disturbs the intrinsic molecular arrangement resulting in a decrease of HTP and a longer helical pitch. Only a few approaches<sup>11,40,41</sup> have been reported on chiral azobenzene dopants in linear geometries such as ones exhibiting more rod-like *Z* forms<sup>40</sup> or cybotactic smectic-like domains which can be dissociated at *Z*-rich state.<sup>41</sup>

In this study, we focused on glycomacrocyces (GM) consisting of sugar and azobenzene as feasible photoresponsive chiral dopants to achieve higher HTP in *Z*-rich state and its significant switching by light irradiation, which have never been utilized to the best of our knowledge. The glycomacrocylic azobenzene derivatives reported by Xie *et al.* are known to undergo a significant conformational change and interesting chiroptical properties upon photoisomerization.<sup>48-50</sup> Transfer of chirality from sugar unit to azobenzene could induce certain helicity preferentially, and single molecular chirality level was well switched between *E* and *Z* forms with high fatigue resistance and thermal stability. In addition, slight variation on linker length or sugar skeleton may bring significant differences in photoinduced geometrical transition and chiroptical properties. Therefore, these attractive features of glycomacrocylic compounds encouraged us to introduce them as novel and powerful photoresponsive chiral dopants to CLC.

Importantly, such an efficient and high degree of helical reorganization can be utilized to perform mechanical work by rotating macroscopic objects on the film. The two (opposite)-directional rotations have been somewhat exploited since Feringa's group demonstrated the first molecular machine showing rotational motion.<sup>29-31</sup> However, single-directional rotational motion is hardly attainable due to the helix winding and unwinding process in opposite direction on the way to each photostationary state (PSS). Recently, our group overcame such issues realizing molecular machinery (crankshaft effect) by implementing rotational stripe patterns and static focal conic domains (FCDs) in CLCs.<sup>35</sup>

Herein, we demonstrate the unique switching behavior of glycomacrocycle-based azobenzene dopants shown in Scheme 1 exhibiting stronger helical twisting induction in the Z-rich state, that is higher HTP (up to 500% empowerment) and shorter helical pitch with  $E \rightarrow Z$  photoisomerization. Theoretical studies were also carried out to reveal the plausible molecular mechanism. In addition, we present herein the first example of the application of glycomacrocylic azobenzene dopants that induce versatile phototunability of rotational mechanical movement, either reversible rotational direction switching or single-directional rotating crankshaft mode of microscopic glass rod on the surface of a CLC mixture film. Eventually, we could propose another promising category of photoresponsive chiral dopants exhibiting amplification of HTP upon  $E \rightarrow Z$  photoisomerization which can devote as molecular machines for macroscopic mechanical work manipulation.



**Scheme 1.** Molecular structures of **1** and **2**, and their photoisomerization upon UV ( $E$  to  $Z$  form) and visible ( $Z$  to  $E$  form) light irradiation.

## 2. RESULTS AND DISCUSSION

### 2.1 Glycomacrocycles affecting phase transition of the LC host

Molecular structures of photoresponsive GM-based azobenzenes and their photoisomerization process upon UV ( $E$  to  $Z$  form) and visible ( $Z$  to  $E$  form) light irradiation are described in Scheme 1. Azobenzene-embedded glycomacrolactones with the photochromic moiety linked to 4,6-position of *manno* (**1**, 17-membered ring) and 2,3-position of *gluco* (**2**, 16-membered ring) derivatives were synthesized<sup>48,49</sup> and utilized. Two

compounds were well dissolved into nematic LC hosts such as 5CB, DON-103, or ZLI-1132 resulting in cholesteric phase. For example, **1** was introduced into 5CB up to 8.5 wt% showing good solubility, and we could observe different phases depending on the doping concentration and upon photoirradiation (Table S1). At the relatively low doping concentration around 1~2 wt%, it exhibited classic Grandjean textures.<sup>1</sup> By elevating the dopant concentration, highly strained FCDs were observed which are known as one of the cholesteric phases. Double spiral FCDs (Figure 1a) and polygonal FCDs (Figure 1b) were distinguished without and with the cover glass, respectively. It is noticeable that the doping concentration around 5 wt% resulted in the photoinduced reversible isotropization of the FCDs upon UV light exposure at room temperature shown as the black region in the polarizing optical microscope (POM) image (Figure 1c and d), and the FCDs were recovered upon thermal back reaction. Further doping at 8.5 wt% afforded an isotropic phase even before photoirradiation (Table S1). Unlike **1**, doping **2** to 5CB at 0.12 wt% showed the chiral phase induction by UV light irradiation. In addition, photoinduced isotropization did not occur even at 8.5 wt% which implies that **2** has higher miscibility and chiral transferability compared to **1**.

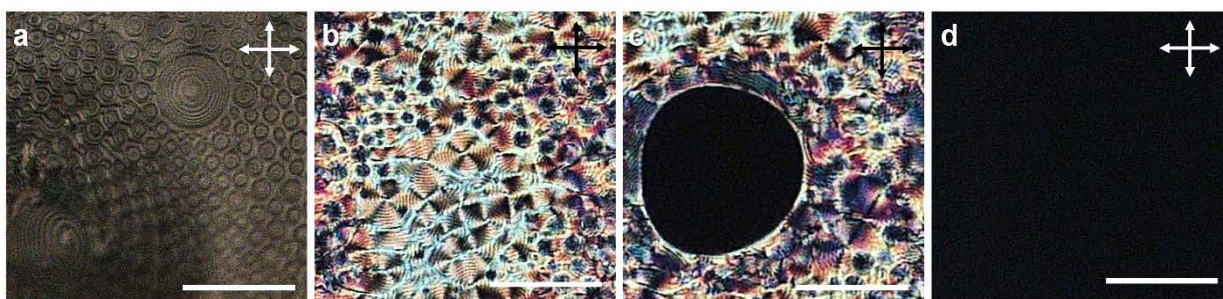


**Figure 1.** Polarizing optical microscope images of CLCs of **1** doped in nematic 5CB (5 wt%) on polyimide-rubbed glass substrate: (a) Open-air film without a cover glass showing double spiral focal conic domains. (b-d) Sandwiched film with cover glass showing focal conic textures; (b) initial and (c, d) upon continuous UV light irradiation exhibiting photoinduced isotropization. White scale bar: 100  $\mu\text{m}$ .

## 2.2 Unprecedented switching of HTPs: larger values for the Z forms

We examined the chirality transfer characteristics of **1** and **2** in CLCs by using Cano's wedge method.<sup>51</sup> Each CLC composite was prepared by mixing the host NLC and the dopant homogeneously, followed by injection into a Grandjean–Cano wedge cell under capillary force at room temperature. As shown in wedge cell images containing CLCs of 4 wt% of **1** in 5CB (a-c) and 1 wt% of **2** in ZLI-1132 (d-f) in Figure 2, clear Cano's lines were observed which represent the formation of the cholesteric orientation of the molecules. Induced  $P_s$  of CLCs and HTP values of the dopants could be determined (see the experimental section for the calculation). Illumination of the wedge cell with UV (365 nm) light and visible (510 nm) light to each PSS brought a dynamic shift of the Cano lines. Interestingly, reversible shortening and lengthening of the distance between the Cano lines occurred upon the irradiation with UV and visible light, respectively. In particular, dramatic gap shrinkage between Cano lines was witnessed from **2** at Z-rich PSS<sub>UV</sub> (Figure 2e) as  $P$  changes about 6 times from 8.4  $\mu\text{m}$  to 1.4  $\mu\text{m}$  reflecting the significant increase in the chirality transferability in Z-form. The residual Z-form at subsequent PSS<sub>vis</sub> inhibited the full restore to the original (*i.e.*, prior to photo-irradiation) pitch length. Table 1 summarizes the  $P_s$  and HTPs of the GM-azo dopants in the nematic LC hosts 5CB, DON-103, and ZLI-1132 before (initial) and after irradiation with UV and visible light to each PSS. In the initial state, the **2**-based CLCs exhibit relatively higher HTPs compare with those of **1** which suggests that **2** would have higher intrinsic chirality and/or better mesogenic compatibility to the nematic LC host. Remarkably, every photoresponsive CLC showed a tendency of an increasing manner of HTP with a large switching ratio ( $\Delta\beta/\beta_{\text{ini}}$ ) over 50 % upon UV light irradiation and its decreasing upon subsequent visible light irradiation. To our surprise, the largest HTP photoswitching from 11.9 to 72.3  $\mu\text{m}^{-1}$ ,  $\Delta\beta/\beta_{\text{ini}}$  of 508 % was obtainable in the presence of **2**. Although rare



cases on *Z*-photoisomerization induced HTP increase have been reported from azobenzene derivatives in linear geometries by Ichimura,<sup>40</sup> Kurihara,<sup>41</sup> and us,<sup>11</sup> such empowering helicity in *Z*-form even in a cyclic geometry is unprecedented for photochromic chiral dopants.

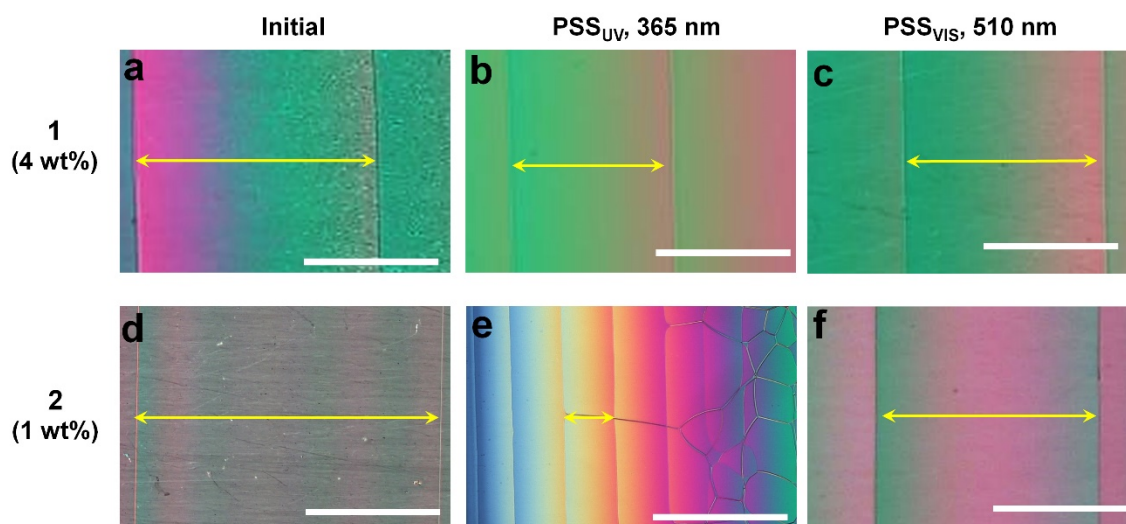


**Figure 2.** Cano wedge cell images with the Cano lines obtained from CLC mixtures containing 4 wt% of **1** in 5CB (a: initial,  $P = 7.4 \mu\text{m}$ , b:  $\text{PSS}_{\text{UV}}$ ,  $P = 4.7 \mu\text{m}$ , c:  $\text{PSS}_{\text{vis}}$ ,  $P = 5.9 \mu\text{m}$ ) and 1 wt% of **2** in ZLI-1132 (d: initial,  $P = 8.4 \mu\text{m}$ , e:  $\text{PSS}_{\text{UV}}$ ,  $P = 1.4 \mu\text{m}$ , f:  $\text{PSS}_{\text{vis}}$ ,  $P = 5.9 \mu\text{m}$ ). White scale bar: 100  $\mu\text{m}$ .

**Table 1.** Photoswitching of the helical twisting power ( $\beta$ ) of CLCs doped with **1** or **2** upon 365 nm ( $E \rightarrow Z$  isomerization) and 510 nm ( $Z \rightarrow E$  isomerization) light irradiation.

Dopant (conc.)	Nematic LC host	Light (PSS)	$P$ ( $\mu\text{m}$ )	$\beta$ ( $\mu\text{m}^{-1}$ )	$ \Delta\beta/\beta_{\text{ini}} $ (%) <sup>a</sup>
<b>1</b> (2 wt%)	5CB	initial	14.9	3.4	+59
		UV	9.3	5.4	
		Vis	11.8	4.2	
	DON-103	initial	34.8	1.4	+93
		UV	18.6	2.7	
		Vis	28.7	1.7	
ZLI-1132	initial	25.0	2.0	+74	

		UV	14.4	3.5	
		Vis	23.5	2.1	
		initial	7.5	13.4	
	5CB	UV	4.5	22.4	+67
		Vis	6.5	15.6	
		initial	27.2	3.7	
	DON-103	UV	11.4	8.7	+135
		Vis	19.5	5.1	
		initial	8.4	11.9	
	ZLI-1132	UV	1.4	72.3	+508
		Vis	5.9	17.0	

<sup>a)</sup> Switching ratio in HTP between the initial ( $\beta_{ini}$ ) and  $PSS_{UV}$  states

### 2.3 Photoregulation of the rotational motion of microsized objects

Motivated by such large HTP photoswitching of the CLCs, we attempted to investigate the light-induced microscale collective motion of the CLC texture and its consequent modulation of mechanical motion of micro-objects freckled on the CLC surface.<sup>35</sup> Firstly, the doped CLC mixture was drop-cast onto a glass substrate coated with a unidirectionally rubbed polyimide alignment film, and was then observed under POM equipped with light sources of 365 nm and 510 nm at room temperature.<sup>34</sup> As shown in Figure 3a, clear stripe-like patterns of CLC (1.7 wt% **2** in 5CB) were observed at the beginning, which is a direct consequence of the cholesteric geometry with lying helix parallel to the substrate at the interface of air and CLC. Interestingly, FCDs were rapidly formed upon UV light irradiation (8 mW cm<sup>-2</sup>) (Figure 3b).

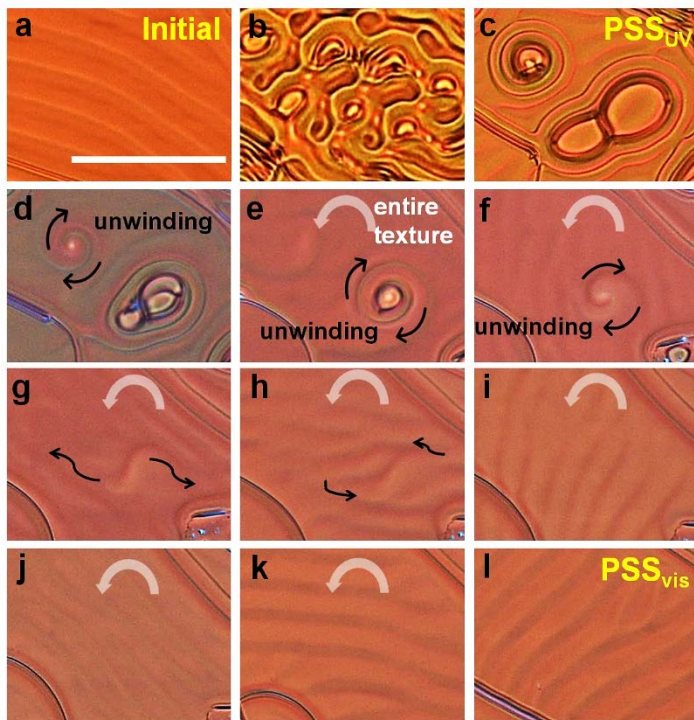


**Figure 3.** Photoinduced CLC film (1.7 wt% **2** in 5CB) surface texture transition: initial stripe-like texture (a), focal conic domains formed by UV light irradiation ( $8 \text{ mW cm}^{-2}$ ) (b), and after reaching  $\text{PSS}_{\text{UV}}$  (c). During visible light irradiation ( $25 \text{ mW cm}^{-2}$ ) from (d) to (l), the helically strained focal conic domains are unwinding in the opposite direction to the entire texture rotation followed by total dissipation (d→g) and fused to the collective counter-clockwise rotation (h→l). White scale bar:  $100 \mu\text{m}$ .

Usually, a FCD comprises multiple domains with an intrinsic helical pitch, with the helical axis of each domain being randomly oriented throughout the surface. Continuous UV light irradiation resulted in the integration of FCDs and simultaneous restore of stripe textures by reaching  $\text{PSS}_{\text{UV}}$ , and we specifically monitored the dissipation process of residual FCDs (Figure 3c-i) upon subsequent visible light irradiation ( $25 \text{ mW cm}^{-2}$ ). We could witness the clockwise unwinding process of the helically strained FCDs in the opposite direction to the entire texture rotation followed by total dissipation (d→g). They were finally fused to the counter-clockwise collective rotation (h), and the homogeneous large domain of a few hundred square micrometer scale showed successive dynamic rotational motion (i→l). The

shape and size of FCDs were quite similar to those observed from our recent study on CLCs doped with planar chiral cyclic azobenzene upon  $Z \rightarrow E$  photoisomerization.<sup>35</sup> Although the FCD formation was triggered by  $E \rightarrow Z$  isomerization in this work which is the opposite manner from the previously reported system, the common feature in two systems is that the FCDs emerged at the HTP switching to a higher value. Therefore, it indicates that a potential “seed” cluster generation in the CLCs inducing disoriented FCDs is likely to be triggered at the HTP increasing step. These disoriented FCDs contain random helical directors with many domain boundaries across the surface of the film which failed to accumulate rotational reorganization of the CLC texture, consequently resulting in no rotation of a small object on the film. In addition, careful observation of the reorganization process from FCDs to homogeneous stripe patterns revealed that the intrinsic helical directors’ orientation in FCDs is independent from homogeneously reorganized stripe-patterns. Consequently, formed stripe patterns and their collective rotational reorganization encouraged us to photochemically drive mechanical rotational motion of a small object.

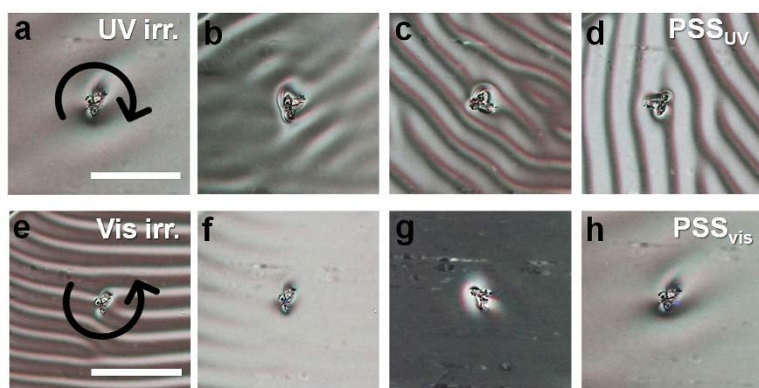


**Figure 4.** Rotational motion of a glass flake on the surface of CLC mixture film (1.4 wt% **1** in 5CB) upon continuous UV light irradiation of low intensity ( $2 \text{ mW cm}^{-2}$ ) from  $\text{PSS}_{\text{vis}}$  (a) to  $\text{PSS}_{\text{UV}}$  (d) in the clockwise direction. Counter-clockwise rotational motion from  $\text{PSS}_{\text{UV}}$  (e) to  $\text{PSS}_{\text{vis}}$  (h) upon visible light irradiation ( $25 \text{ mW cm}^{-2}$ ). White scale bar:  $100 \mu\text{m}$ .

Utilizing the unprecedented large HTP switching characteristics of **1** and **2**, we tried to

realize the rotational movement of micro-objects generated by the photoinduced rotation of stripe textures. Micro-sized objects such as glass flakes or rods were sprinkled on the surface of CLC film followed by UV and the subsequent visible light irradiation. Figure 4 and Figure 5 demonstrate the photoinduced rotational motion behavior of glass flakes monitored with **1** doped CLC (1.4 wt% in 5CB). The UV light irradiation was controlled for low ( $2 \text{ mW cm}^{-2}$ ) and high- ( $8 \text{ mW cm}^{-2}$ ) intensity while the identical intensity of visible light ( $25 \text{ mW cm}^{-2}$ ) was utilized. Interestingly, upon low-intensity UV irradiation, a clockwise rotation of both homogeneous stripe textures and the glass flake was observed, instead of the emergence of FCDs (Figure 4a-d). Meanwhile, counter-clockwise rotational movement of the texture and the glass flake was observed upon subsequent visible light irradiation (Figure 4e-h). The rotational angle until reaching  $\text{PSS}_{\text{UV}}$  and  $\text{PSS}_{\text{vis}}$  was about  $320^\circ \pm 50^\circ$ . By contrast, upon high intensity UV light irradiation, instant generation of FCDs was observed (Figure 5b). Continuous UV light irradiation resulted in the steady restore of the original stripe texture, but imperfect retaining some domain boundaries (Figure 5e). Thus, unfortunately, upon visible light exposure from  $\text{PSS}_{\text{UV}}$ , it hardly exhibited rotational motion of the glass flake although minor rotational reorganization of the stripe texture inside the boundaries was observed (Figure 5f-i).

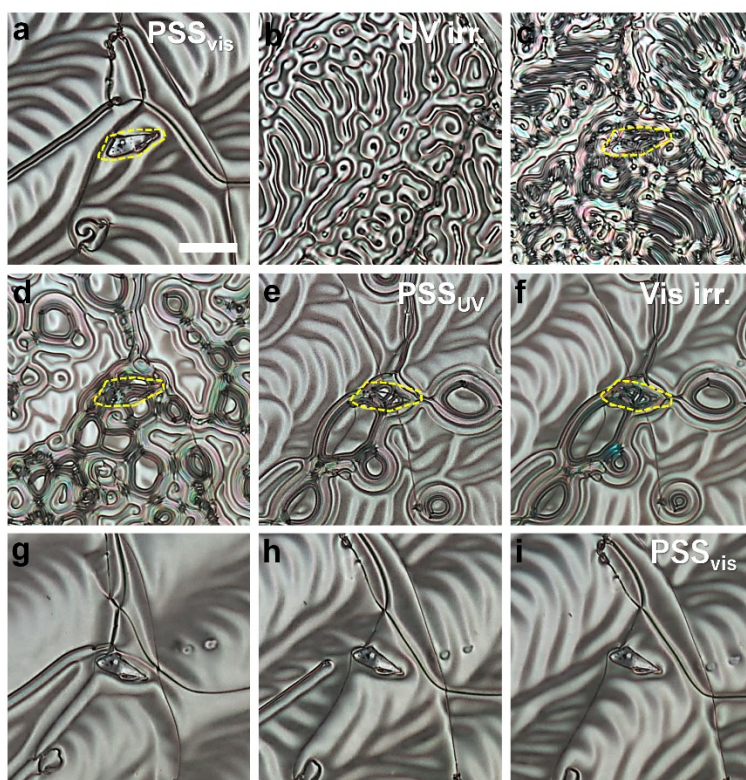


**Figure 5.** Images of a glass flake on the surface of CLC mixture film (1.4 wt% **1** in 5CB) upon UV light irradiation of full intensity ( $8 \text{ mW cm}^{-2}$ ) from initial  $\text{PSS}_{\text{vis}}$  (a) to  $\text{PSS}_{\text{UV}}$  (e). Subsequent visible light irradiation ( $25 \text{ m Wcm}^{-2}$ ) to  $\text{PSS}_{\text{vis}}$  (i). White scale bar:  $100 \mu\text{m}$ .

Afterward, we examined the photoinduced rotational motion behaviour of **2**-doped CLCs (1.7 wt% in 5CB). We could confirm the quite improved rotational movement of the glass flake compared with that of CLC doped with **1**. Firstly, low-intensity UV light and subsequent visible light irradiation resulted in the clockwise and counter-clockwise rotation in  $415^\circ \pm 10^\circ$  which is larger than that observed from **1** (see Figure S1). This dynamic motion was much amplified when introducing ZLI-1132 (doping 1 wt% of **2**) which showed the largest HTP switching ratio (Table 1). Larger rotation angles of  $570^\circ$  (clockwise) and  $640^\circ$  (counter-clockwise) was obtained from  $\text{PSS}_{\text{UV}}$  (a→d) and  $\text{PSS}_{\text{vis}}$  (e→h), respectively (Figure 6). The difference in the resultant rotational angles depending on the CLCs is thought to be reasonable considering the one of the critical parameters which determines the degree of

rotation reorganization is known to be the photoinduced HTP switching ratio.<sup>8,27</sup> Meanwhile, unidirectional rotational motion of a glass flake was obtained in which only counter-clockwise rotational motion was realized on the surface of CLC mixture film (1.7 wt% of **2** in 5CB) upon consecutive full intensity UV and visible light irradiation (Figure 7). Intense UV irradiation resulted in the paused state of the micro-object due to the emergence of the dense FCDs (Figure 7b). Randomly oriented helix with many domain boundaries in FCDs failed to amplify discrete rotational reorganization of each independent domain in CLC film. This static state retained till  $PSS_{UV}$  (Figure 7e), in the meantime the homogeneous stripe textures were recovered which is similar to the one in the initial state. Accumulation of rotational angle by repetitive unidirectional rotational motion is demonstrated in Figure 7. Upon two rounds of alternating UV and visible light irradiation, the glass flake showed non-rotating static state upon the first (a→e) and the second (j→l) UV irradiating step, then counter-clockwise rotational motion was observed upon the first (f→i) and the second (m→o) visible light irradiating step exhibiting rotation angles of  $310^\circ$  and  $340^\circ$ , respectively. Accordingly, photo-controlled reversible supramolecular reorganization of CLC confirmed as a transition between stripe texture and focal conic texture led to the multiple cycles of object rotation in one-way. The delivered mechanical work is not canceled out by reverse movement. The summarized rotation behavior from **1**- and **2**-based CLCs at each light irradiation condition is shown in Table S2.

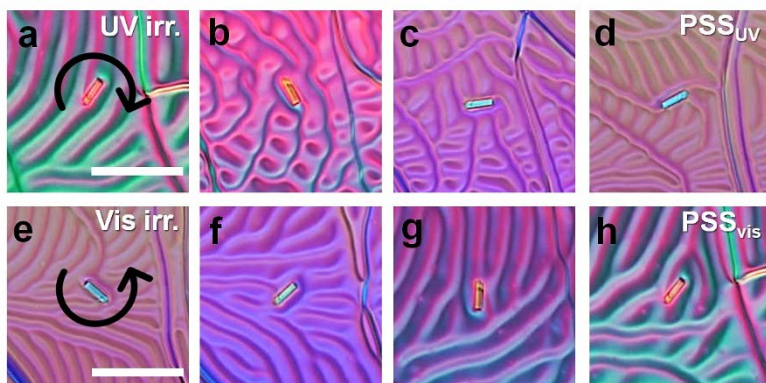


**Figure 6.** Rotational motion of a glass rod on the surface of the CLC mixture film (1 wt% **2** in ZLI-1173) upon continuous UV light irradiation of low intensity ( $2 \text{ mW cm}^{-2}$ ) starting from  $\text{PSS}_{\text{vis}}$  (a) to  $\text{PSS}_{\text{UV}}$  (e) exhibiting  $570^\circ$  in the clockwise direction. Counter-clockwise rotational motion from  $\text{PSS}_{\text{UV}}$  (e) to  $\text{PSS}_{\text{vis}}$  (h) upon visible light irradiation ( $25 \text{ mW cm}^{-2}$ ) exhibiting  $640^\circ$ . White scale bar:  $100 \mu\text{m}$ .

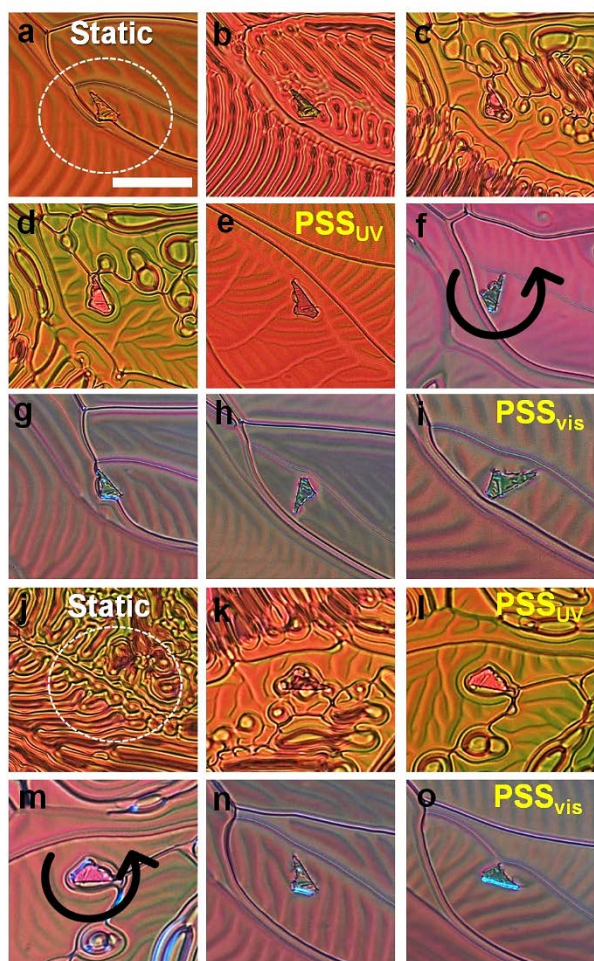


**Figure 7.** Unidirectional rotational motion of a glass flake on the surface of CLC mixture



film (1.7 wt% of **2** in 5CB) upon two rounds of alternating UV (full intensity, 8 mW cm<sup>-2</sup>) and visible light (25 mW cm<sup>-2</sup>) irradiation. It showed non-rotating static state upon the first (a→e) and the second (j→l) UV irradiating step. Counter-clockwise rotational motion was observed upon the first (f→i) and the second (m→o) visible light irradiating step exhibiting rotation angles of 310° and 340°, respectively. White scale bar: 100 μm.

As the photoinduced HTP switching and the resultant texture transition of CLC depend on not only the isomer ratio of the dopants but also the orientation of molecules, we examined the *E-Z* isomer ratios in CLCs at each photostationary state quantitatively by <sup>1</sup>H NMR (Table S3) and their UV-vis absorbance transitions (Figure 8). Photoconversion ratios of **1** and **2** in CLC films utilized for rotational motion demonstration were varied 80~84% (*Z*) at PSS<sub>UV</sub> and 47~56% (*E*) at PSS<sub>vis</sub>. The compounds showed comparable or slightly lower *E*→*Z* conversions in LCs compared in MeCN<sup>49</sup> at PSS<sub>UV</sub>. By contrast, they exhibited higher *Z*→*E* conversions in LCs than in MeCN (upon 514 nm light irradiation) at PSS<sub>vis</sub>. This implies the LC medium effect is plausibly valid to promote *Z*→*E* photoconversion, which is very interesting and requires further investigation. Meanwhile, difference of *E/Z* conversion ratio between ZLI-1132 and 5CB doped with **2** was small while they exhibited significantly different HTP photoswitching ratio. Therefore, we presume that the difference in conformational compatibility of *E* and *Z* isomers with LC molecules and their orientations would play an important role to determine the photoinduced cholesteric reorganization.

The UV-Vis absorption spectra of CLC films exhibiting FCDs are shown in Figure 8. Verifying the π-π\* band transition of **1** and **2** led us to understand the UV light-induced FCD formation and dissociation phenomenon. Basically, maximum absorbance is obtained when the electric field of the incident light and the directions of π-π\* transition moment of molecules are parallel to each other. If molecules are tilted from their parallel position, they cannot effectively absorb the light resulting in the decrease of the absorption. In our previous

study,<sup>35</sup> we could reveal that the CLC with stripe textures has relatively high absorbance originated from the homogeneous helical director with hybrid anchoring (molecules align parallel to the substrate at the interface of air and perpendicular in the bulk), while photoinduced FCDs are likely to have randomly oriented helix with many domain boundaries resulting in absorbance decrease. In Figure 8, absorption band centered at 352 nm is assigned to  $\pi$ - $\pi^*$  transition of *E*-form moiety. Irradiation with UV light onto the film showed the decrease of the absorption band intensity caused by *E*→*Z* photoisomerization. It is noteworthy that the absorbance instantly decreased reaching its minimum for initial 15 s of irradiation. With continuous UV light irradiation, the absorbance gradually increased and saturated at  $PSS_{UV}$ . This unusual absorption drop shown at 352 nm is possibly ascribed to the drastically formed disoriented FCDs. As the domains were gradually reorganized again to recover the alignment close to original stripe texture upon continuous UV-exposure, absorbance was increased. Subsequent 510 nm light irradiation ( $PSS_{vis}$ ) resulted in further recovery of  $\pi$ - $\pi^*$  absorption band intensity centered at 352 nm because of *Z*→*E* photoisomerization. Although **1** and **2** dopants exhibited similar *Z*:*E* isomer ratio in 5CB (Table S3) and spectral transition behavior, higher absorption band recovery at  $PSS_{vis}$  was witnessed for **2**-doped CLC film (Figure 8b) compared to that of **1** (Figure 8a). This suggests that a higher degree of reorientation in **2**-doped CLC enabled to repeat the unidirectional rotational motions shown in Figure 7.

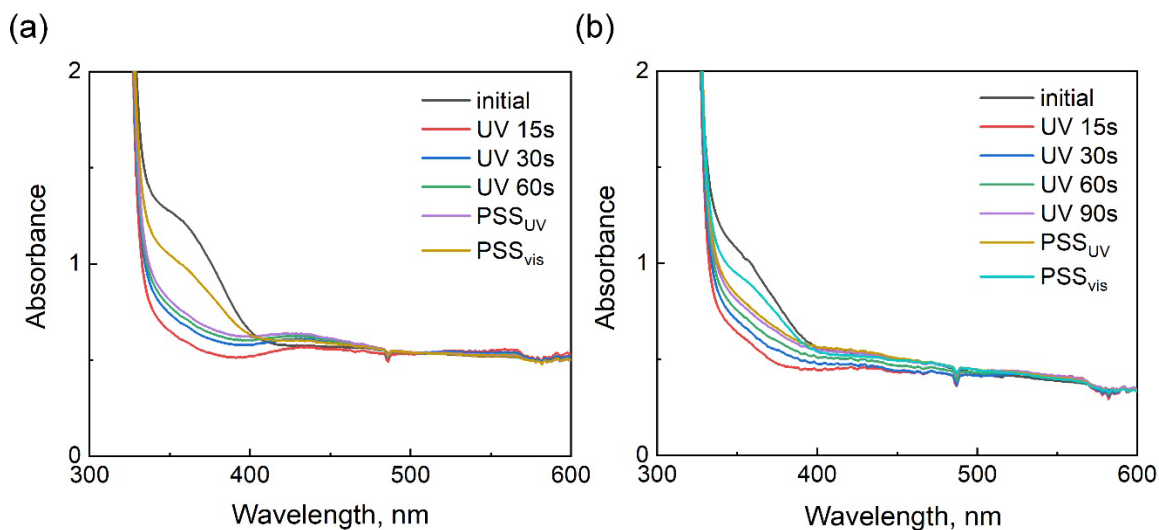


**Figure 8.** UV-visible absorption spectra of a CLC film doped with (a) **1** (1.4 wt% in 5CB) and (b) **2** (1.7 wt% in 5CB) upon UV and visible light irradiation.

To gain more insights into the molecular orientations, order parameter ( $S$ ) was obtained from the polarization absorption spectra of those CLC films according to the equation,  $S=(A_{\parallel}-A_{\perp})/(A_{\parallel}+2A_{\perp})$ , where  $A_{\parallel}$  and  $A_{\perp}$  are the absorbance measured at 342 nm when the polarization of an incident light was parallel or perpendicular to the long axis of LC molecules, respectively. Initial state  $S$  was identical (0.04), but  $PSS_{UV}$  exhibited increasing manner of  $S$  values as 0.11 and 0.20 for **1**- and **2**-based CLCs, respectively. Subsequent visible light irradiation resulted in their decrease to 0.07 and 0.10 for **1** and **2** at  $PSS_{vis}$ , respectively (Table S4). Judging from the photoinduced transition in absorption spectra and  $S$  of CLC films, we could conclude that less oriented CLCs doped with *E*-isomers contributed to the formation of randomly oriented FCDs at the early stage of UV light irradiation. Upon UV light exposure, the *E* isomers relatively in random alignment in LC were replaced with *Z*-isomers, then those seed clusters expanded resulting in FCDs with many boundaries across the surface of the film. It lacks the momentum of rotational reorganization of the LC texture and thereby caused no rotation of the macroscopic object on the film. However, as the *E*→*Z* photoisomerization

proceeded, the higher miscibility of *Z*-isomers with nematic host was likely to promote the orientation of LC molecules to achieve higher molecular orientation and HTP values. In the meantime, domains were gradually reorganized again to form a homogeneous and original stripe texture which is ready to drive the rotational motion again upon subsequent *Z*→*E* isomerization of **2**. In contrast, we failed to mechanically rotate the object on the film containing **1** due to the partial reorganization into stripe texture at  $PSS_{UV}$ . Remaining grain boundaries would inhibit the collective motion which turned out to be insufficient to rotate the object. The detailed molecular mechanism is discussed in the next section.

Besides, it is noteworthy that UV irradiation intensity control gave an obvious difference in the cholesteric texture transition behavior. By decreasing the UV light intensity, a smaller number of FCDs emerged with fading grain boundaries. At certain point (i.e. 1/4 of its full UV intensity), FCD was not formed anymore but the texture and micro-object underwent the clockwise rotational motion as observed in Figures 4 and 6 for **1** and **2**, respectively. It means that the seed clusters for FCDs can be photo-controlled. Suppressing disoriented seed clusters expansion was enabled by the gradual helical reorganization upon moderate *E*→*Z* isomerization which also promoted helices re-aligning to afford homogeneous stripe textures concomitantly.

#### 2.4 Geometry study of **1** and **2**

The dopant chirality transfer to the NLC proceeds through molecular scale solvent-solute interactions. It implies that the *E*→*Z* photoisomerization of azobenzene unit of **2** could effectively improve intramolecular and intermolecular-supramolecular level interactions which leads to much favorable geometry for chirality transfer. Experimental results shown in Figure 9 represent the absorption (top) and CD spectra (bottom) of *E* (left) and *Z* (at  $PSS_{365}$ ,

right) isomers of **1** (blue) and **2** (yellow) in CH<sub>3</sub>CN. The overlapped regions are in green. For both the *manno* macrolactone (**1**) and the *gluco* macrolactone (**2**), the CD spectra showed Cotton effect with a negative band at 454 nm and a positive band (350 nm) corresponding respectively to n→π\* and π→π\* transitions of the azobenzene in acetonitrile. Irradiation at 365 nm led to a blue shift of all CD bands, without sign reversal or significant change in intensity. **2** exhibited more intense CD signals both in *E* and *Z* forms compared with those of **1** which suggests a higher potential for helicity induction of **2**.

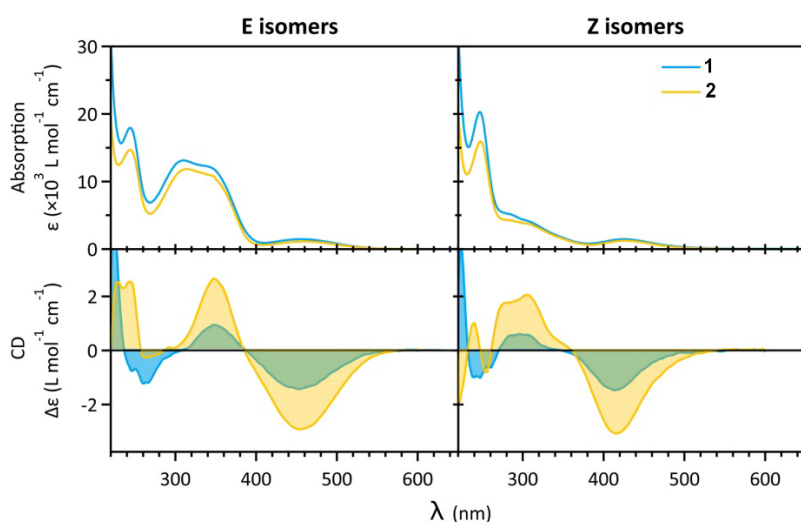
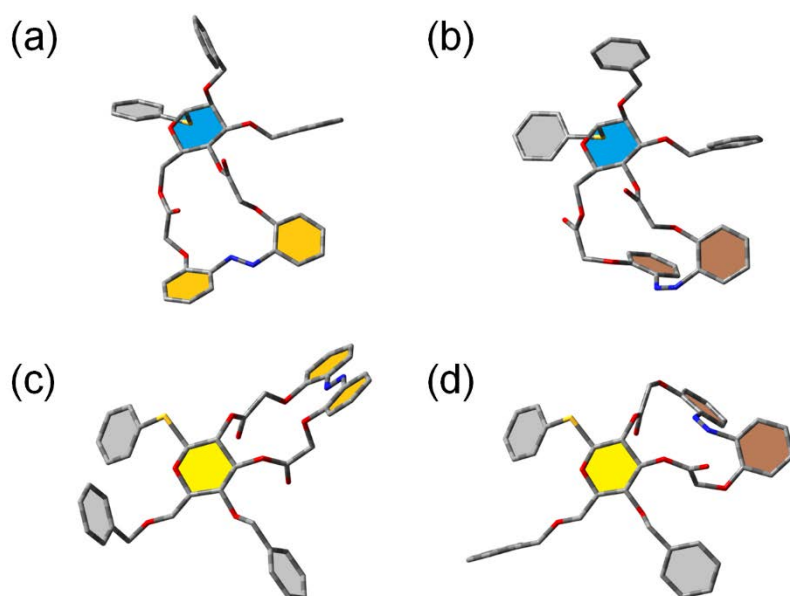


**Figure 9.** Experimental absorption (top) and CD spectra (bottom) of *E* (left) and *Z* (at PSS<sub>365</sub>, right) isomers of **1** (blue) and **2** (yellow) in CH<sub>3</sub>CN. The overlapped regions are in green.

It has been reported that azobenzene could generate *P* or *M* helical chirality. After a DFT geometry optimization of *E*- and *Z*-(*P*),(*M*) of macrocycles **1** and **2** by using respectively B3LYP and PBE0/6-311G functional and basis set, the TD-DFT calculations indicate that *E*-(*P*) and *Z*-(*P*) exhibit a negative first Cotton-effect pattern whereas *E*-(*M*) and *Z*-(*M*) display a positive first Cotton-effect pattern. Therefore, comparison of experimental and simulated CD spectra indicates that *E*- and *Z*-forms adopt preferentially a (*P*) configuration as shown in Figure 9.<sup>48,49</sup>

Herein, we reported the comparison of the DFT calculations<sup>52</sup> using PBE0/6-311G+(d,p)

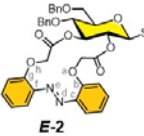
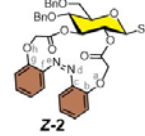
as level of theory for both compounds (Figure 10, Table 2 and Table S5). The N=N double bond (C-N=N-C) was chosen as a representative dihedral angle of the torsion in the macrocycles, which is about +12.7° to +10.5° for *Z*-(*P*) of **1** and **2**, respectively, and close to -180° for *E*-(*P*) of both **1** and **2** (Table 2). The planes of the phenyl ring are twisted around the N=N-C planes for all structures. Low torsional angles of C-N=N-C for *Z*-(*P*) may somewhat contribute to the improved miscibility with nematic host molecules to achieve higher HTP values upon *E*→*Z* photoisomerization.



**Figure 10.** Calculated geometries of (a) *E*-(*P*)-**1**, (b) *Z*-(*P*)-**1**, (c) *E*-(*P*)-**2**, (d) *Z*-(*P*)-**2** (PBE0/6-311G+(d,p) in vacuum).

**Table 2.** Dihedral angles obtained by DFT (PBE0/6-311G+(d,p)) calculations in the azobenzene moieties of the macrocycles with a (*P*) helicity.

	Isomers	Dihedral angles $\xi$ (°)				
		C-N=N-C $\overline{cdef}$	C=C-N=N $\overline{bcde}$	N=N-C=C $\overline{defg}$	[O-C <sub>q</sub> ]-[O-C <sub>q</sub> ] $\overline{abgh}$	[C-C]-[C-C] $\overline{bcfg}$
	<i>E</i> - <b>1</b>	-177.7	12.61	159.99	50.03	37.53
	<i>Z</i> - <b>1</b>	12.7	59.8	-139.7	-29.4	-26.2

		<b>E-2</b>	-179.9	-170.1	-6.5	3.2	7.9
		<b>Z-2</b>	10.5	-176.2	-128.4	67.4	132.8

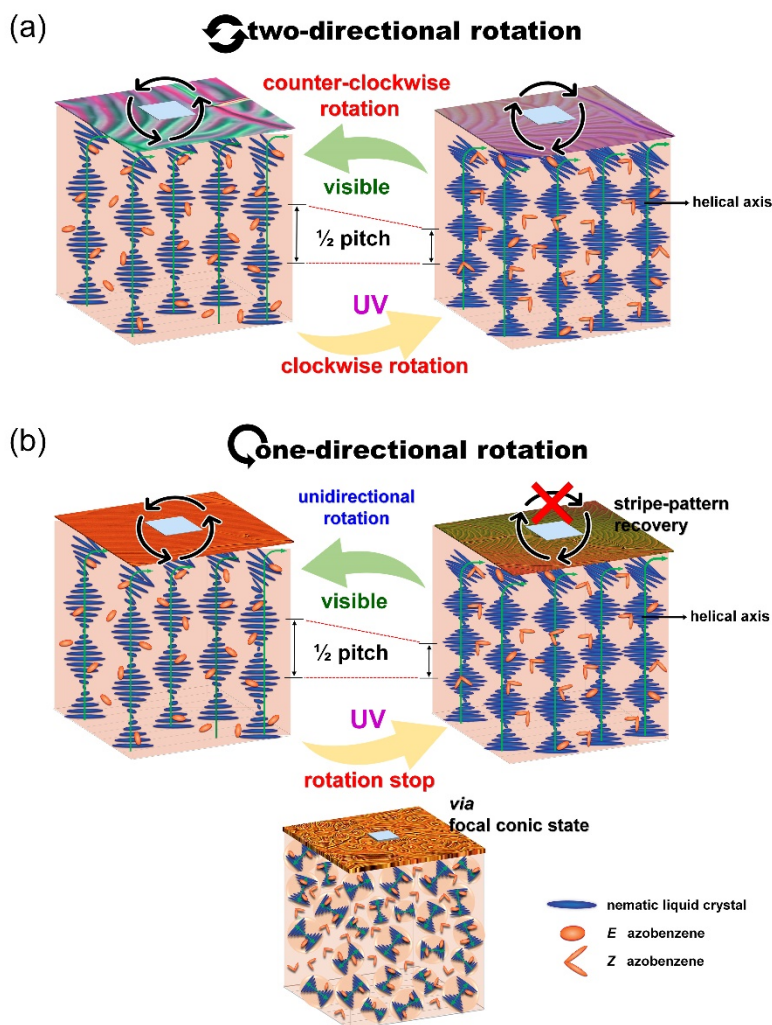
According to the previous study of Xie *et al.*,<sup>49</sup> the  $E \rightarrow Z$  photoisomerization of glycomacrocycles followed by  $^1\text{H}$  NMR showed that  $E$ - and  $Z$ -isomers display distinct NMR signals due to the large conformational change induced by isomerization. Interestingly, the sugar  $^4\text{C}_1$  chair conformation remains unchanged whatever the  $E$  or  $Z$  isomers of *gluco* or *manno* derivatives, while downfield shifts for sugar protons in the macrocycle **1** and large shift of  $-\text{OCH}_2\text{CO}-$  protons involved in the cyclic structure of compounds **1** and **2** have been observed. In addition, theoretically obtained intramolecular distances of the azobenzene and sugar moieties in  $E$  and  $Z$  forms (Table S5) provide us another plausible clue for the photoinduced-chirality transfer characteristics of two dopants. A larger intramolecular distance of **E-1** than that of **E-2** was observed due to the longer linker unit of **E-1**. Upon  $E \rightarrow Z$  photoisomerization, those intramolecular distances show a larger difference. While **1** has minor transition below  $0.3 \text{ \AA}$ , **2** shows  $1.6\text{--}2.2 \text{ \AA}$  of significant decrement associated with the higher ring strain in its  $Z$ -form, benefiting superstructural chirality transfer. Thus, experimentally observed unique HTP switching manner (large increment upon  $E \rightarrow Z$  photoisomerization) of the dopant is understandable considering the geometrical change.

Besides, these geometry transitions of the dopants influence the cholesteric texture reorganization behavior for rotational motion induction. **1** is geometrically less compatible with nematic host molecules (less mesogenic) due to the larger macrocyclic cavity size. In addition, as **E-1** undergoes somewhat moderate photoinduced geometrical transition compared with **E-2**, FCDs formed upon UV light irradiation would have a lower chance for helical reorganization during the subsequent  $Z \rightarrow E$  photoisomerization. Eventually, the

coexistence of remaining grain boundaries from FCDs and partially restored stripe texture inhibits the collective rotational motion of texture and the micro-objects (Figure 5). Whereas large photoinduced conformational change and the smaller cavity with strong ring strain of **2** exhibiting relatively favorable compatibility with nematic host molecules (improved mesogenic property) could possibly facilitate the domain reorganization process which resulted in the reversible cholesteric texture switching and amplified rotational motion of the micro-object (Figures 3 and 7).

The schematic demonstration (Scheme 2) summarizes the plausible effect of  $E \leftrightarrow Z$  photoisomerization of macrocyclic azobenzene dopant **2** on the photoinduced chiral superstructural reorganization with higher HTP (pitch decrement) upon *Z*-rich state, and in case of undergoing two-directional or unidirectional one-way rotation of glass flakes upon UV (clockwise rotation or stop) and visible light (counter-clockwise rotation) irradiation. This particular system meets the requirements or criteria to be considered as real molecular machinery implementing a molecular crankshaft effect<sup>35</sup> which can continuously utilize the external energy to perform mechanical work by using the molecular switching mechanism.





**Scheme 2.** Schematic representation of the plausible effect of *E/Z* photoisomerization of macrocyclic azobenzene dopant **2** on the photoinduced chiral superstructural reorganization with higher HTP (pitch decrement) in the *Z*-rich state, undergoing (a) two-directional rotation and (b) one-directional rotation of the glass flakes upon UV and visible light irradiation.

### 3. CONCLUSION

In conclusion, we demonstrated that CLCs doped with glycomacrocylic azobenzene derivatives exhibit an unprecedented switching manner of HTP and cholesteric texture transition upon UV and visible light irradiation. Larger HTP (highly strained helix or shorter pitch length) in the *Z*-rich state than that in the *E*-state was observed upon UV light irradiation, which is hardly attainable in common azobenzene dopants based on CLC system.

In addition, tuning the UV light intensity irradiated to CLC film resulted in two kinds of cholesteric textures: homogeneous stripes or focal conics. Therefore, we could demonstrate the two rotational motion modes of micro-object floated on the CLC film: reversible or unidirectional rotational motion, which were triggered by the dynamic collective reorganization of the cholesteric texture. The underlying molecular mechanism could be estimated with a theoretical geometry study on glycomacrocylic azobenzene dopants. It is highly anticipated that the novel molecular system can be exploited to provide versatile phototunabilities of mechanical work.

## **EXPERIMENTAL SECTION**

The synthesis of **1** and **2** is described in refs 48,49. The NLC host 5CB was purchased from Kanto Chemical Co. Inc. (Japan), and DON-103 and ZLI-1132 were obtained from DIC Corporation (Japan) and Merck, respectively. All other solvents and chemicals were purchased from commercial sources and used without further purification. Micro glass rods and flakes were purchased from Nippon Electric Glass. Photoisomerization was conducted using 365 nm (2-8 mW cm<sup>-2</sup>) and 510 nm (25 mW cm<sup>-2</sup>) LED light sources from Hayasaka-Rikoh Co. Microscopic analyses were performed using an Olympus BX-60 optical microscope equipped with Moticam1080, Shimadzu Rika Co. UV-Vis spectrophotometer (Agilent 8453) was utilized to confirm the absorption spectra of CLC films. Every measurement was conducted at room temperature. Geometry optimizations were performed by DFT using the PBE0 exchange functional. The basis set 6-311G+(d,p) has been chosen in vacuum, implemented in the Gaussian09 software package.<sup>52</sup> The absence of negative frequencies was checked to ensure true minima for all geometries.

## **Supporting Information**

The Supporting Information is available free of charge on the ACS Publications website. Methods for the measurement of helical pitch length, HTP ( $\beta$ ) and *E-Z* isomer ratio of CLCs. Rotational motion of CLC containing 1.7 wt% **2** in 5CB upon UV light irradiation of low intensity and visible light irradiation. A table on doping concentration-dependent phase transition of **1** in nematic 5CB. A table on summary of rotation behavior of micro-objects from **1** and **2** doped CLCs. A table on *E-Z* isomer ratio measured at PSS<sub>UV</sub> and PSS<sub>vis</sub>. A table on order parameter (*S*) of CLC films at initial, PSS<sub>UV</sub> and PSS<sub>vis</sub>. A table on intramolecular distances (Å) between the azobenzene and sugar moieties determined from the obtained optimized geometries by DFT calculations (PBE0/6-311G+(d,p)).

### **Corresponding Author**

\*E-mail: ykim@es.hokudai.ac.jp; tamaoki@es.hokudai.ac.jp; joanne.xie@ens-paris-saclay.fr

### **Author Contributions**

The manuscript was written through contributions of all authors. All authors have given approval to the final version of the manuscript.

### **ACKNOWLEDGMENT**

The theoretical investigation was performed using HPC resources from the “Mésocentre” computing center of CentraleSupélec and École Normale Supérieure Paris-Saclay supported by CNRS and Région Île-de-France (<http://mesocentre.centralesupelec.fr/>). YK acknowledges the partial financial support from Mazda Foundation, JSPS Grants-in-Aid for Scientific Research KAKENHI (JP16K17886 and 19K05624) and Core-to-Core Program. The support of the president grant for promoting overseas research and education exchange and WinGS Global Networking Awards from Hokkaido University is appreciated. The

support from the Network Joint Research Centre for Materials and Devices as well as the Dynamic Alliance for Open Innovation Bridging Human, Environment and Materials from MEXT is acknowledged.

## REFERENCES

- (1) Bisoyi, H. K.; Li, Q. Light-Driven Liquid Crystalline Materials: From Photo-Induced Phase Transitions and Property Modulations to Applications. *Chem. Rev.* **2016**, *116*, 15089-15166.
- (2) Lv, J.; Liu, Y.; Wei, J.; Chen, E.; Qin, L.; Yu, Y. Photocontrol of Fluid Slugs in Liquid Crystal Polymer Microactuators. *Nature* **2016**, *537*, 179-184.
- (3) Ikeda, T.; Mamiya J.-I.; Yu, Y. Photomechanics of Liquid-Crystalline Elastomers and Other Polymers. *Angew. Chem. Int. Ed.* **2007**, *46*, 506-528.
- (4) Yu, H. Recent Advances In Photoresponsive Liquid-Crystalline Polymers Containing Azobenzene Chromophores. *J. Mater. Chem. C* **2014**, *2*, 3047-3054.
- (5) Mukai, K.; Imai, K.; Hara, M.; Nagano, S.; Seki, T. A High - Density Azobenzene Side Chain Polymer Brush for Azimuthal and Zenithal Orientational Photoswitching of A Nematic Liquid Crystal. *Chemphotochem* **2019**, *3*, 495-500.
- (6) Li, J.; Bisoyi, H. K.; Lin, S.; Guo, J.; Li, Q. 1,2-Dithienyldicyanoethene-Based, Visible-Light-Driven, Chiral Fluorescent Molecular Switch: Rewritable Multimodal Photonic Devices, *Angew. Chem. Int. Ed.* **2019**, *58*, 16052-16056.
- (7) Kim, Y.; Mafy, N. N.; Tamaoki, N. *Photoactive Functional Soft Materials: Photochemical Chirality Induction and Inversion in Soft Materials*, 2019 Wiley-VCH (Eds. Q. Li.).
- (8) Kim, Y.; Tamaoki, N. Photoresponsive Chiral Dopants: Light-Driven Helicity Manipulation in Cholesteric Liquid Crystals for Optical and Mechanical Functions. *Chemphotochem* **2019**, *3*, 284-303.
- (9) Mathews, M.; Tamaoki, N. Reversibly Tunable Helicity Induction and Inversion in Liquid Crystal Self-Assembly by a Planar Chiroptic Trigger Molecule. *Chem. Commun.* **2009**, 3609-3611.

- (10) Kim, Y.; Tamaoki, N. A Photoresponsive Planar Chiral Azobenzene Dopant with High Helical Twisting Power. *J. Mater. Chem. C* **2014**, *2*, 9258-9264.
- (11) Kim, Y.; Tamaoki, N. Asymmetric Dimers of Chiral Azobenzene Dopants Exhibiting Unusual Helical Twisting Power upon Photoswitching in Cholesteric Liquid Crystals. *ACS Appl. Mater. Interfaces* **2016**, *8*, 4918-4926.
- (12) Bisoyi H. K.; Bunning T. J.; Li Q. Stimuli-Driven Control of the Helical Axis of Self-Organized Soft Helical Superstructures. *Adv Mater.* **2018**, *30*, 1706512 (1-35).
- (13) Wang, H.; Bisoyi H. K.; Li, B. X.; McConney, M. E.; Bunning T. J.; Li, Q. Visible-Light-Driven Halogen Bond Donor Based Molecular Switches: From Reversible Unwinding to Handedness Inversion in Self-Organized Soft Helical Superstructures, *Angew. Chem. Int. Ed.* **2020**, *59*, 2684-2687.
- (14) Wang, H.; Bisoyi, H. K.; McConney, M. E.; Urbas, A. M.; Bunning, T. J.; Li, Q. Visible-Light-Induced Self-Organized Helical Superstructure in Orientationally Ordered Fluids, *Adv. Mater.* **2019**, *31*, 1902958 (2-6).
- (15) Bisoyi, H. K.; Li, Q. Light-Directing Chiral Liquid Crystal Nanostructures: From 1D to 3D. *Acc. Chem. Res.* **2014**, *47*, 3184-3195.
- (16) Wu, S. T.; Yang, D. K. *Reflective Liquid Crystal Displays*, John Wiley & Sons, 2001.
- (17) Mathews, M.; Tamaoki, N. Planar Chiral Azobenzenophanes as Chiroptic Switches for Photon Mode Reversible Reflection Color Control in Induced Chiral Nematic Liquid Crystals. *J. Am. Chem. Soc.* **2008**, *130*, 11409-11416.
- (18) Mitov, M. Cholesteric Liquid Crystals with A Broad Light Reflection Band. *Adv. Mater.* **2012**, *24*, 6260-6276.
- (19) Fan, J.; Li, Y.; Bisoyi, H. K.; Zola, R. S.; Yang, D.-K.; Bunning, T. J.; Weitz, D. A.; Li, Q. Light-Directing Omnidirectional Circularly Polarized Reflection from Liquid Crystal Droplets. *Angew. Chem. Int. Ed.* **2015**, *54*, 2160-2164.
- (20) Wang, L.; Dong, H.; Li, Y.; Xue, C.; Sun, L.-D.; Yan, C.-H.; Li, Q. Reversible Near-Infrared Light Directed Reflection in a Self-Organized Helical Superstructure Loaded with Upconversion Nanoparticles. *J. Am. Chem. Soc.* **2014**, *136*, 4480-4483.
- (21) Zheng, Z.-G.; Li, Y.; Bisoyi, H.; Wang, L.; Bunning, T. J.; Li, Q. Three-Dimensional Control of the Helical Axis of a Chiral Nematic Liquid Crystal by Light. *Nature* **2016**, *531*, 352-356.

- (22) Ma, L. L.; Duan, W.; Tang, M. J.; Chen, L. J.; Liang, X.; Lu, Y. Q.; Hu, W. Light-Driven Rotation and Pitch Tuning of Self-Organized Cholesteric Gratings Formed in a Semi-Free Film. *Polymers* **2017**, *9*, 295.
- (23) Qin, L.; Gu, W.; Wei, J.; Yu, Y. Piecewise Phototuning of Self-Organized Helical Superstructures. *Adv. Mater.* **2018**, *30*, 1704941.
- (24) Tamaoki, N. Cholesteric Liquid Crystals for Color Information Technology. *Adv. Mater.* **2001**, *13*, 1135-1147.
- (25) Coles, H.; Morris, S. M. Liquid-Crystal Lasers. *Nature Photon.* **2010**, *4*, 676-685.
- (26) Chen, L.; Li, Y.; Fan, J.; Bisoyi, H. K.; Weitz, D. A.; Li, Q. Photoresponsive Monodisperse Cholesteric Liquid Crystalline Microshells for Tunable Omnidirectional Lasing Enabled by a Visible Light-Driven Chiral Molecular Switch. *Adv. Opt. Mater.* **2014**, *2*, 845-848.
- (27) Thomas, R.; Yoshida, Y.; Akasaka, T.; Tamaoki, N. Influence of a Change in Helical Twisting Power of Photoresponsive Chiral Dopants on Rotational Manipulation of Micro Objects on the Surface of Chiral Nematic Liquid Crystalline Films. *Chem. Eur. J.* **2012**, *18*, 12337-12348.
- (28) Kausar, A.; Nagano, H.; Kuwahara, Y.; Ogata, T.; Kurihara, S. Photocontrolled Manipulation of a Microscale Object: A Rotational or Translational Mechanism. *Chem. Eur. J.* **2011**, *17*, 508-515.
- (29) Eelkema, R.; Pollard, M. M.; Vicario, J.; Katsonis, N.; Ramon, B. S.; Bastiaansen, C. W.; Broer, D. J.; Feringa, B. L. Molecular Machines: Nanomotor Rotates Microscale Objects. *Nature* **2006**, *440*, 123.
- (30) Eelkema, R.; Pollard, M. M.; Katsonis, N.; Vicario, J.; Broer, D. J.; Feringa, B. L. Rotational Reorganization of Doped Cholesteric Liquid Crystalline Films. *J. Am. Chem. Soc.* **2006**, *128*, 14397-14407.
- (31) Bosco, A.; Jongejan, M. G. M.; Eelkema, R.; Katsonis, N.; Lacaze, E.; Ferrarini, A.; Feringa, B. L. Photoinduced Reorganization of Motor-Doped Chiral Liquid Crystals: Bridging Molecular Isomerization and Texture Rotation. *J. Am. Chem. Soc.* **2008**, *130*, 14615-14624.
- (32) Wang, Y.; Li, Q. Light-Driven Chiral Molecular Switches or Motors in Liquid Crystals. *Adv. Mater.* **2012**, *24*, 1926-1945.

- (33) Delden, R. A. Van; Mecca, T.; Rosini, C.; Feringa, B. L. A Chiroptical Molecular Switch with Distinct Chiral and Photochromic Entities and its Application in Optical Switching of a Cholesteric Liquid Crystal. *Chem. Eur. J.* **2004**, *10*, 61-70.
- (34) Kim, Y.; Frigoli, M.; Vanthuyne, N.; Tamaoki, N. A Helical Naphthopyran Dopant for Photoresponsive Cholesteric Liquid Crystals. *Chem. Commun.* **2017**, *53*, 200-203.
- (35) Mafy, N. N.; Kim, Y.; Thomas, R.; Akasaka, T.; Tamaoki, N. Molecular Crankshaft Effect Converting Piston-Like Molecular Motion to Continuous Rotation of Macro Objects. *ACS Appl. Mater. Interfaces* **2019**, *11*, 15097-15102.
- (36) Lancia, F.; Yamamoto, T.; Ryabchun, A.; Yamaguchi, T.; Sano, M.; Katsonis, N. Reorientation Behavior in the Helical Motility of Light-Responsive Spiral Droplets. *Nat. Commun.* **2019**, *10*, 5238.
- (37) Orlova, T.; Lancia, F.; Loussert, C.; Iamsaard, S.; Katsonis, N.; Brasselet, E. Revolving Supramolecular Chiral Structures Powered by Light in Nanomotor-Doped Liquid Crystals. *Nat. Nanotech.* **2018**, *13*, 304-308.
- (38) Nakagawa, T.; Ubukata, T.; Yokoyama, Y. Chirality and Stereoselectivity in Photochromic Reactions. *J. Photochem. Photobiol. C* **2018**, *34*, 152-191.
- (39) Eelkema, R.; Feringa, B. L. Amplification of Chirality in Liquid Crystals. *Org. Biomol. Chem.* **2006**, *4*, 3729-3745.
- (40) Ruslim, C.; Ichimura, K. Conformation-Assisted Amplification of Chirality Transfer of Chiral Z-Azobenzenes. *Adv. Mater.* **2001**, *13*, 37-40.
- (41) Yoshioka, T.; Ogata, T.; Nonaka, T.; Moritsugu, M.; Kim, S.-N.; Kurihara, S. Reversible- Photon-Mode Full-Color Display by Means of Photochemical Modulation of a Helically Cholesteric Structure. *Adv. Mater.* **2005**, *17*, 1226-1229.
- (42) Kawamoto, M.; Aoki, T.; Wada, T. Light-Driven Twisting Behaviour of Chiral Cyclic Compounds. *Chem. Commun.* **2007**, 930-932.
- (43) Gottarelli, G.; Hibert, M.; Samori, B.; Solladie, G.; Spada, G. P.; Zimmermann, R. Induction of the Cholesteric Mesophase in Nematic Liquid Crystals: Mechanism and Application to the Determination of Bridged Biaryl Configurations. *J. Am. Chem. Soc.* **1983**, *105*, 7318-7321.
- (44) Matteo, A. Di; Todd, S. M.; Gottarelli, G.; Solladié, G.; Williams, V. E.; Lemieux, R. P.; Ferrarini, A.; Spada, G. P. Correlation Between Molecular Structure and Helicity

- of Induced Chiral Nematics in Terms of Short-Range and Electrostatic-Induction Interactions. The Case of Chiral Biphenyls. *J. Am. Chem. Soc.* **2001**, *123*, 7842-7851.
- (45) Mathews, M.; Zola, R. S.; Hurley, S.; Yang, D.-K.; White, T. J.; Bunning, T. J.; Li, Q. Light-Driven Reversible Handedness Inversion in Self-Organized Helical Superstructures *J. Am. Chem. Soc.* **2010**, *132*, 18361-18366.
- (46) Nishikawa, H.; Mochizuki, D.; Higuchi, H.; Okumura, Y.; Kikuchi, H.; Reversible Broad-Spectrum Control of Selective Reflections of Chiral Nematic Phases by Closed-/Open-Type Axially Chiral Azo Dopants. *Chemistryopen* **2017**, *6*, 710-720.
- (47) Lu, H. B.; Xie, X. Y.; Xing, J.; Xu, C.; Wu, Z. Q.; Zhang, G. B.; Lv, G. Q.; Qiu, L. Z. Wavelength-Tuning and Band-Broadening of a Cholesteric Liquid Crystal Induced by a Cyclic Chiral Azobenzene Compound. *Opt. Mater. Exp.* **2016**, *6*, 3145-3158.
- (48) Lin, C.; Maisonneuve, S.; Metivier, R.; Xie, J. Photoswitchable Carbohydrate-Based Macrocyclic Azobenzene: Synthesis, Chiroptical Switching, and Multistimuli-Responsive Self-Assembly. *Chem. Eur. J.* **2017**, *23*, 14996-15001.
- (49) Lin, C.; Maisonneuve, S.; Theulier, C.; Xie, J. Synthesis and Photochromic Properties of Azobenzene-Derived Glycomacrolactones. *Eur. J. Org. Chem.* **2019**, 1770-1777.
- (50) Lin, C.; Jiao, J.; Maisonneuve, S.; Mallétoit, J.; Xie, J. Stereoselective Synthesis and Properties of Glycoazobenzene Macrocycles Through Intramolecular Glycosylation. *Chem. Commun.* **2020**, *56*, 3261-3264.
- (51) Cano, R. An Explanation of Grandjean Discontinuities. *Bull. Soc. Fr. Mineral.* **1968**, *91*, 20-27.
- (52) Frisch, M. J.; Trucks, G. W.; Schlegel, H. B.; Scuseria, G. E.; Robb, M. A.; Cheeseman, J. R.; Scalmani, G.; Barone, V.; Petersson, G. A.; Nakatsuji, H.; Li, X.; Caricato, M.; Marenich, A. V.; Bloino, J.; Janesko, B. G.; Gomperts, R.; Mennucci, B.; Hratchian, H. P.; Ortiz, J. V.; Izmaylov, A. F.; Sonnenberg, J. L.; Williams-Young, D.; Ding, F.; Lipparini, F.; Egidi, F.; Goings, J.; Peng, B.; Petrone, A.; Henderson, T.; Ranasinghe, D.; Zakrzewski, V. G.; Gao, J.; Rega, N.; Zheng, G.; Liang, W.; Hada, M.; Ehara, M.; Toyota, K.; Fukuda, R.; Hasegawa, J.; Ishida, M.; Nakajima, T.; Honda, Y.; Kitao, O.; Nakai, H.; Vreven, T.; Throssell, K.; Montgomery, J. A., Jr.; Peralta, J. E.; Ogliaro, F.; Bearpark, M. J.; Heyd, J. J.; Brothers, E. N.; Kudin, K. N.; Staroverov, V. N.; Keith, T. A.; Kobayashi, R.;



Normand, J.; Raghavachari, K.; Rendell, A. P.; Burant, J. C.; Iyengar, S. S.; Tomasi, J.; Cossi, M.; Millam, J. M.; Klene, M.; Adamo, C.; Cammi, R.; Ochterski, J. W.; Martin, R. L.; Morokuma, K.; Farkas, O.; Foresman, J. B.; Fox, D. J. Gaussian 09, Revision A.02, Gaussian, Inc., Wallington CT, 2016.

## Table of Contents

